Response of underground cable duct systems to travelling seismic waves

W. Blair Gohl
Pacific Geodynamics Inc.

Takashi Kojima
BC Hydro

W. Scott Dunbar
Dept. of Mining & Mineral Process Engineering, University of B.C.

Michael K. Lee
BC Hydro

Abstract: Finite element models were applied to estimate the dynamic response of buried cable duct systems to travelling seismic waves representative of earthquake ground motions in the Lower Mainland of British Columbia. The purpose of the modelling was to study whether or not power cables installed in ducts buried in non-liquefiable ground in the BC Hydro transmission system are at risk of disengaging at joint connectors under seismic conditions. This paper presents the method of analysis, including modelling of external duct - soil interaction and internal duct - cable sliding interaction, and identification of significant factors which affect the dynamic response of cables to travelling seismic waves. The modelling suggested that in some cases, excessive forces could be set up in the cables at manhole entrances depending on characteristics of the input ground motions, cable properties and installation conditions, and if sufficient slack is not provided in the cable.

Introduction

Finite element models were developed to estimate the dynamic response of underground transmission cables installed in pipes and ducts to representative earthquake ground motions in the Lower Mainland of British Columbia. The purpose of the modelling was to study whether or not cable duct systems which are installed in non-liquefiable ground in the BC Hydro transmission system are at risk of developing large tensile forces and disengaging at joint connectors under seismic conditions. This paper presents the method of analysis and identifies significant factors which affect the dynamic response of cables to travelling seismic waves. The effect of liquefaction-induced, large ground displacement acting on the cable is not considered in the present analysis.

Cable Duct Configurations

The cables are housed in buried ducts encased in concrete or in steel pipes (see Fig. 1). A typical single conductor oil filled (SCOF) cable utilizes three of four ducts (one is a spare duct) arranged in a square configuration and encased in concrete. For high pressure pipe type (HPOF) cables, three individual cables are installed in a steel pipe.

Fig. 1. Cross-sections showing configurations of cables in ducts and pipes.

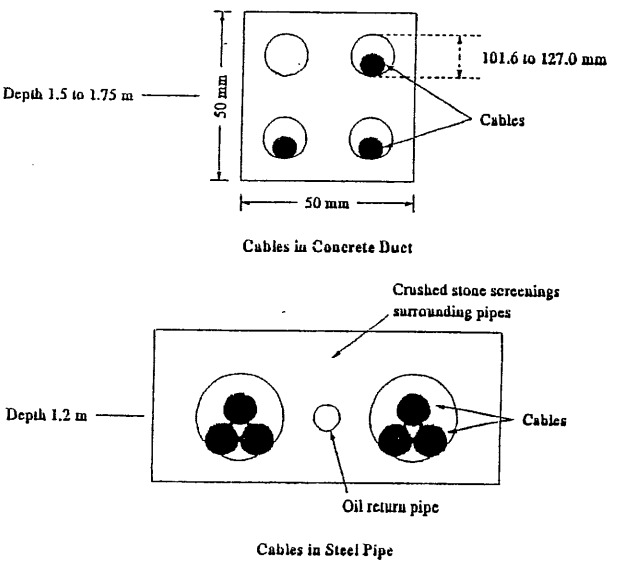

The cable ducts are buried in an excavated trench backfilled with medium dense sand or crushed stone screenings. Burial depths of the cables generally vary between 1 and 3 m. The cables are installed in sections and the length of each section is up to 700 m. The cables may lie on horizontal or sloping ground.

The cables are joined together in manholes at the ends of each section. In the duct system, the ducts end at the manhole walls. The cables of one section exit from each duct and are attached to the cables of the next section by joints mounted on racks attached to the manhole walls. The cables in the manholes are installed with slack to accommodate thermal expansion and contraction of the cable. In the pipe system, the cables and joints are placed in a larger diameter pipe within the manhole.

Analysis Methodology

The analysis methodology divides the cable-duct-soil backfill system into two parts, external and internal, as shown in Fig. 2. The external model consists of the cable duct (steel pipe or concrete duct bank), the cables in the duct, the manhole and the soil backfill surrounding the duct and manhole. The internal model consists of the cable(s) in the duct, and the joints at the manhole. The analyses were carried out using the computer program DRAIN-2DX which is capable of modelling linear and nonlinear, static and dynamic response of complex structural models (Prakash et al, 1993).

External Problem

The finite element model used to represent the external soil-structure interaction problem is shown in Fig. 3. The purpose of the external model is to determine the response of the duct to free field displacement time histories imposed by travelling seismic waves. The displacement output of the external model is then used as input into the internal model which is used to determine the forces within the cable system and at manhole connection joints.

The matrix differential equation solved in the external analysis is:

$$[1] \quad \mathbf{Mu} + \mathbf{Cu} + \mathbf{Ku} = K_s \mathbf{I} u_g$$

where **u** is a vector of the total (absolute) axial displacements at the nodes of the model, **M** is the mass matrix, **C** is the damping matrix, **K** is the axial stiffness matrix of the cable duct (or pipe), **I** is the identity matrix and u_g is a time-dependent vector of input ground displacements at each node.

For external analyses, K_s is the stiffness of the spring used to represent the interaction between the cable duct (or pipe) and the soil. Nonlinear behaviour of the cable duct is incorporated in the stiffness matrix **K** and non-linear soil-duct interaction is incorporated in the spring stiffness, K_s.

Fig. 2. Division of cable-duct/soil system into external and internal models.

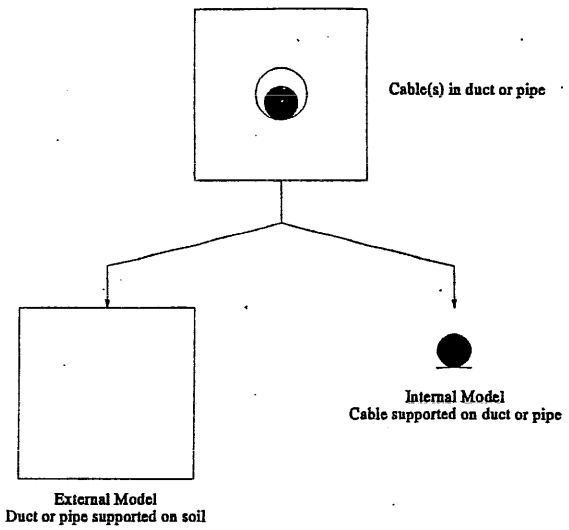

Fig. 3. Finite element model of the cable duct or pipe section used for external analysis.

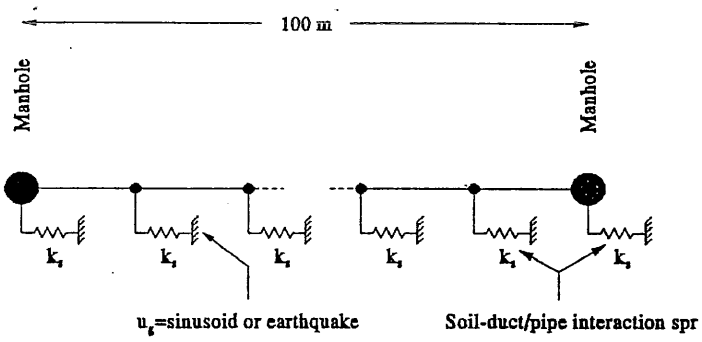

The properties of the soil-duct interaction elements were computed using non-linear axial "t-z" curves described in Audibert et al (1984). Elastic-perfectly plastic t-z curves were adopted with elastic unloading response, resulting in hysteretic behaviour. The large surface area of the manholes at either end of the duct (or pipe) create additional spring stiffness and increase the elastic stiffness and yield force of the interaction springs.

Masses were lumped at each node. A large mass was placed at each end of the model to model the concrete manhole. The mass at other nodes represents the mass of the duct, including the cables. A set of trial geometrical and material properties of the axial bar elements used to represent the duct were provided by BC Hydro. The length of the duct or pipe was assumed to be 100 m for the external analysis.

Stiffness proportional damping was also incorporated, given by $\mathbf{C} = \beta \mathbf{K}$, where $\beta = T_1 \xi / \pi$, T_1 is the fundamental period of the model and ξ is the desired fraction of critical structural damping (0.05 usually). The purpose of such damping is to attenuate high frequencies in the response.

It is possible to incorporate both axial and bending stiffness of duct (or pipe) elements in the above **K** matrix. However, axial displacements of the duct largely dominate axial forces in the internal cables and for this reason we have focused on analysis of axial response of the system. Analyses of flexible cables on horizontal ground subjected to combined axial and lateral (vertical) ground motions showed that the two motions were uncoupled and that small bending moments, much less than the yield moments of the cables, were induced by the levels of lateral ground motion considered. For cables on sloping ground, the two motions are not uncoupled and input of lateral ground motion may be expected to have a small effect on axial forces in the cable. This effect has been neglected in the analyses described.

Internal Problem

The finite element model used to represent the internal soil-structure interaction problem is shown in Fig.4. The same differential equation of motion (equation [1]) is used to solve the problem, incorporating ground displacement time histories derived from the external analysis. The model uses non-linear, bi-directional springs placed along the cable to model cable-duct (or pipe) interaction and nonlinear tension springs (with or without the presence of an initial gap or "slack") to model interaction between the cable entering the manhole and the manhole connector (see Figure 4).

The characteristics of the bi-directional springs used to model cable-duct interaction are developed based on the following considerations. The point at which the cable slides along the duct depends on the ground motion input, which is assumed to be horizontal, the mass of the cable per unit length η, the ground slope θ on which the cable is placed, and the assumed coefficient of friction μ between the cable and the pipe. Referring to Fig.5, the resisting force per unit length parallel to the slope is given by:

$$[2] \quad f_r = \mu \eta g (\cos \theta - a \sin \theta)$$

where g is the acceleration of gravity and (- a) is the ratio of the upslope ground acceleration to g. The driving force per unit length parallel to the slope is due to the weight of the cable and the magnitude of downslope (+a) acceleration given by:

$$[3] \quad f_d = \eta g (\sin \theta + a \cos \theta)$$

Sliding occurs when $f_r = f_d$ leading to a critical acceleration a_c given by:

$$[4] \quad a_c = \pm \frac{\mu \cos \theta - \sin \theta}{\mu \sin \theta + \cos \theta}$$

Downslope or upslope movement of the cable occurs when the resisting force is exceeded. Since there are two values of a_c, there are two corresponding yield forces, one for downslope movement, f_y^+, and one for upslope movement, f_y^-:

$$[5] \quad f_y^+ = \mu \eta g (\cos \theta - a_c \sin \theta)$$

$$[6] \quad f_y^- = \mu \eta g (\cos \theta + a_c \sin \theta)$$

The nonlinear springs are assumed to have an elastic-perfectly plastic response with an initial slope per metre length of cable = 1000 f_y^+ (i.e. assuming a required relative slip displacement between the cable and duct equal to 0.001 m and working in MPa and metre units). The plastic limit of each spring depends on the direction of movement and is governed by either f_y^+ or f_y^-. The spring elements were assumed to unload following their initial elastic slope, resulting in a hysteretic response.

Fig. 4. Finite element model of cable-duct interaction for internal analysis.

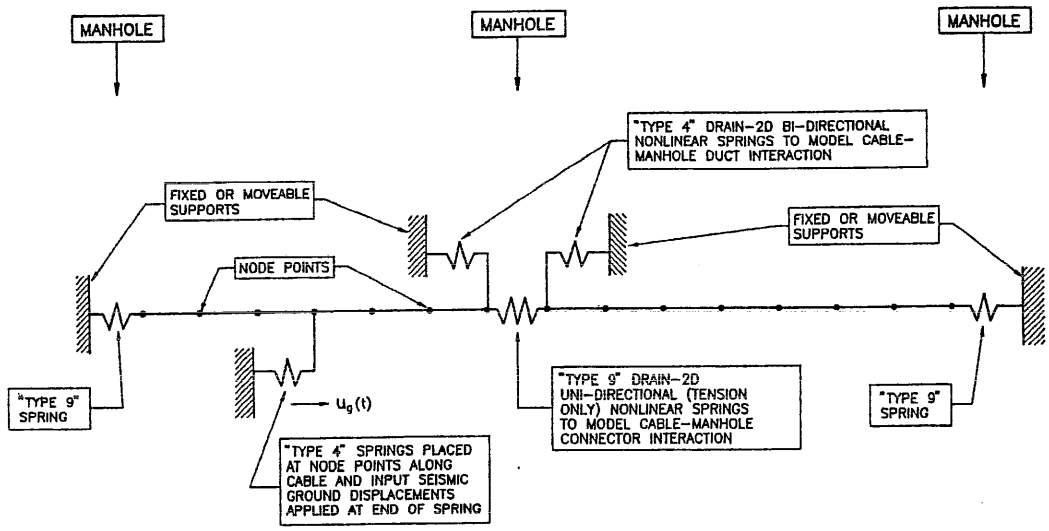

The amplitude of the ground motions applied to the free field end of the manhole connector may be influenced by the mass and geometry of the manhole. For most of the analyses carried out, the mass of the manhole has been assumed not to affect the motion of the cable entering the manhole.Analyses have also been carried out where the free field end of the manhole connector is assumed to be fixed in space and not to be affected by the seismic wave train. This assumes that the manhole completely resists the travelling ground waves.

Fig. 5. Sliding interaction between internal cable and cable duct (or pipe).

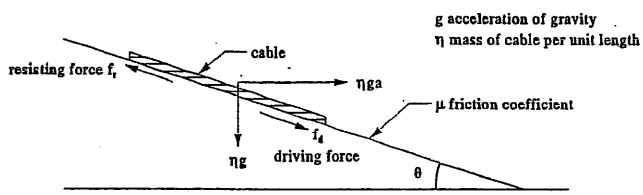

The effect of the weight of the cable acting in the downslope direction is modelled by applying a series of gravity forces at various locations along the cable prior to the start of seismic shaking. These forces are in addition to the induced dynamic forces, which create a bias for cable movement in the downslope direction during shaking. The force per unit length of cable is given by:

[7] $f_x = \eta\, g \sin\theta$

Horizontal displacement time histories are input at the rigid base of the spring interaction elements.

Ground Motion Input

Two earthquake displacement time histories were initially used as input for the analysis of external cable duct-soil interaction. One was the NS component of the displacement time history computed from the corresponding accelerogram recorded at Griffith Park Observatory during the 1971 San Fernando, Ca. earthquake (moment magnitude 6.4). The accelerogram was recorded at a distance of 17 km from the closest point on the fault rupture. The NS component had a peak acceleration of 0.18 g and a peak displacement of 73 mm. The displacements contained a dominant 1 Hz frequency. The second record was the N266E component displacement time history computed from an accelerogram recorded at Olympia, Wa. during the 1949 (moment magnitude 7.1) earthquake. The Olympia N266E component had a peak acceleration of 0.28 g and a peak displacement of 76 mm. The displacements contained a dominant frequency of less than 0.5 Hz. The displacement time histories are shown in Fig.6.

Fig. 6. Displacement time histories used as input from San Fernando, Ca. and Olympia, Wa. earthquake records.

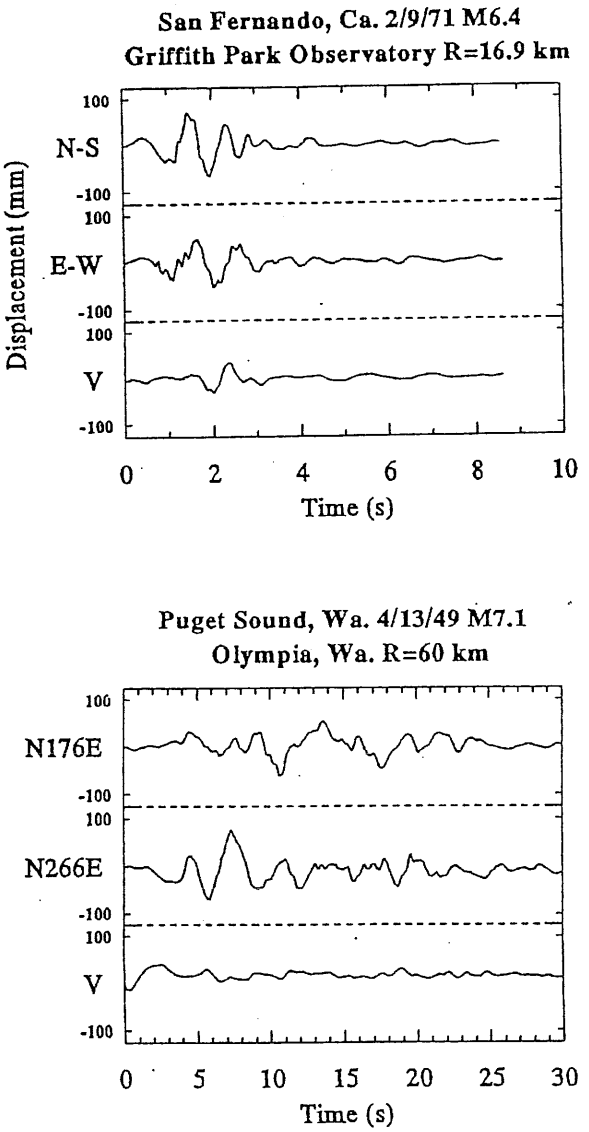

Input displacement time histories used in the analyses were also obtained from accelerograms recorded at the SMART accelerograph array near the city of Lotung in Taiwan. The accelerometer array consists of 37 accelerometers arranged in three concentric circular rings covering an area of approximately 12 sq.km. Since its installation the array has recorded accelerograms due to several earthquakes which occurred in the region. Three component (north-south, east-west and vertical) accelerograms were recorded at each of the accelerometers during a M7.8 earthquake ("Event 45") which occurred approximately 80 km south of the array centre in November, 1986. The corresponding displacement time histories were obtained by integration of the acceleration time histories following application of baseline and instrument corrections. The displacement time histories were supplied by Dr. Bruce Bolt of the University of California, Berkeley.

The north-south displacement components along a line of accelerometers within the array are shown in Fig.7. The peak displacement amplitudes range between 70 and 100 mm. The corresponding peak acceleration amplitudes range between 0.10 g and 0.19 g. Most of the motion is low frequency (0.3 Hz) surface waves propagating across the array. The apparent propagation velocity of the high amplitude surface wave motion is 2800 m/sec. The SMART array time histories were used in the internal cable analyses presented.

Fig. 7. Displacement time histories used as input from SMART array, Event 45, north-south displacement components at various stations.

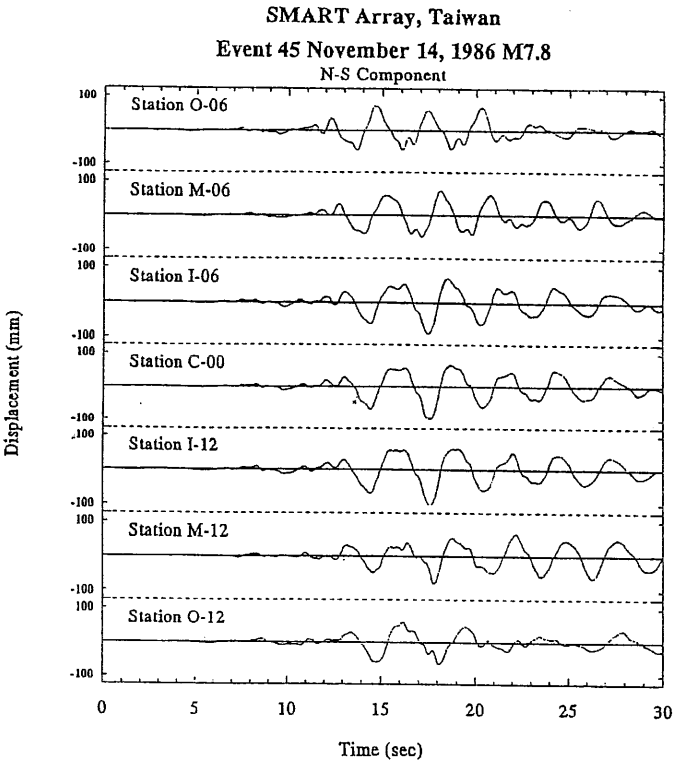

Results of Analysis

External Problem

A series of analyses was conducted to determine the response of a 100 m long, horizontal concrete duct bank or steel pipe to travelling seismic waves inducing axial motion of the duct. Manhole-soil interaction was simplistically modelled using a single mass-spring system. This may not adequately simulate

seismically induced movements of the manhole. The purpose of this analysis was to determine the validity of using the input "free field" ground motion without modification in the internal analysis of the cable. Total axial displacements at various locations along the duct were computed and compared to the input ground motions.

Free field ground displacements from the San Fernando, Ca. and Olympia, Wa. earthquake records were input at the ends of the nonlinear, soil-duct interaction springs and suitably lagged in time to simulate the effect of seismic wave propagation along the cable. In order to assess the possible time lag of input ground motions along the duct bank, a literature review was carried out to estimate the propagation velocities of shear and surface waves measured during previous earthquakes using arrays of accelerometers. Several analyses of the SMART array data have been carried out (Loh, 1985; Hao et al, 1989) which indicated that for 1 to 2 Hz shear wave propagation, the propagation velocity was about 2 km/sec. A review of S-wave propagation velocities carried out by O'Rourke and El Hmadi (1988) for several earthquakes in Japan and the U.S. indicated apparent propagation velocities in the range of 2 to 5 km/sec. Hadjian and Hadley (1981), using data from accelerometer arrays in southern California, found lower bound shear wave propagation velocities of 1 km/sec. The above data were obtained for a range of rock and soil sites.

The propagation velocity of surface waves is a function of the shear wave velocity distribution versus depth and is a function of wavelength of the surface wave, a phenomenon known as dispersion. The longer the wavelength of the propagating surface wave, the deeper the wave travels within the earth. Since soil/rock stiffness and shear wave velocities generally increase with depth, the longer the wavelength the higher the propagation velocity. According to the quarter wavelength phenomenon, a surface wave having a wavelength equal to 4 times the manhole separation distance (=100 m), this will cause the maximum differential displacement along the cable duct. Assuming that the dominant frequencies (f) contained within the earthquake displacement records examined are less than 1 Hz (periods of 1 second or longer), then the minimum propagation value of interest would be given by $c = f\lambda = 400$ m/sec. Data from the SMART array suggests higher surface wave propagation velocities due to the fact that the surface waves recorded were dominated by wave trains having much longer wave lengths than assumed above.

From the above review, we have assumed apparent propagation velocities in the range of 1 to 4 km/sec to simulate travelling wave effects on the cable duct system.

The response of a 100 m long concrete duct incorporating an elastic-plastic stress-strain response and different strengths in tension and compression was next considered. The duct was assumed to be surrounded by medium dense sand. The San Fernando time history was input at two propagation velocities: c=1000 m/sec and c=4000 m/sec. The resulting axial displacement time histories at 20 m intervals along the duct are shown in Fig.8. Yielding of the soil-duct interaction springs and the concrete duct occurred for both propagation velocities. For the case c=1000 m/sec, concrete yielding (cracking) occurred between stations x=20 m and x=40 m. This caused an offset in the computed displacement response following 2 seconds. However, no amplification of the input motions was evident for either case.

The Olympia, Wa. earthquake time history was also input using the same two propagation velocities. The resulting displacement time histories are shown in Fig.9. Yielding of the soil-duct interaction springs occurred for both propagation velocities. No yielding of the concrete duct occurred and no amplification of the input ground motion was evident.

The concrete duct is unreinforced in order to prevent heating due to electromagnetic induction effects when the cable transmits current. Tension cracking of the concrete is therefore a potential concern. However, the phenomenon is based on the results using the San Fernando record which contained a dominant frequency of 1 Hz and assumed a low value of propagation velocity (c=1000 m/sec). The latter tends to emphasize out of phase motions along the duct. Given uncertainties in the ground motion input and in other model parameters, it is difficult to draw a general conclusion regarding the significance of concrete cracking in the model.

Similar analyses were run considering a steel pipe cable duct using the two input ground motions and propagation velocities. The displacement results are shown plotted in Figs. 10 and 11. The pipe did not exhibit yielding although yielding of the soil backfill was found to occur. A limited amount of ground motion amplification occurred for the case c=4000 m/sec and no amplification for c=1000 m/sec.

Whether amplification occurs depends on the changing fundamental frequency of the soil - duct system relative to the dominant frequencies within the input ground motion. The fundamental frequency and its change with time depends on backfill stiffness and strength properties. For amplification to occur, the ground motion must be long enough for the critical frequencies to excite the structure. This is less likely for random earthquake motions and suggests it is reasonable to assume ground displacements applied to the internal cables are equal to those in the free field.

Fig. 8. Concrete duct axial displacement response to the San Fernando earthquake displacement time history at equally spaced locations along a 100 m duct section and considering two propagation velocities. The zero lag (x=0) input time history is also shown.

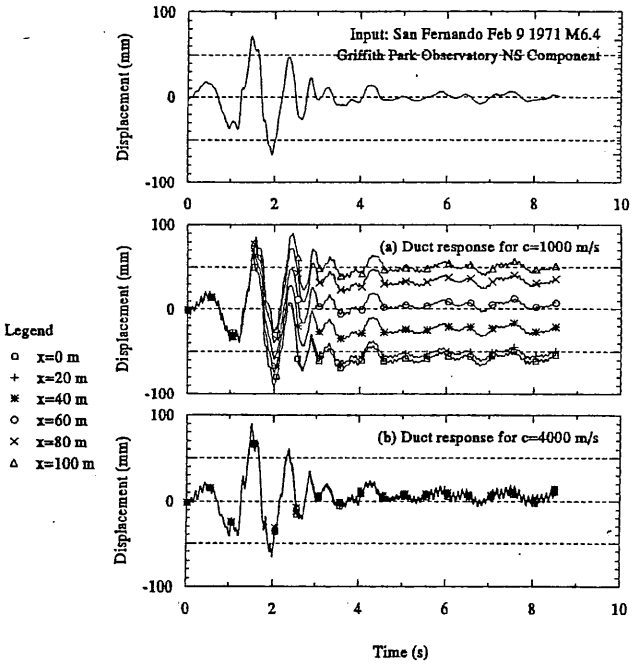

Fig. 9. Concrete duct axial displacement response to the Olympia, Wa. earthquake displacement time history at equally spaced locations along a 100 m duct section and considering two propagation velocities. The zero lag (x=0) input time history is also shown.

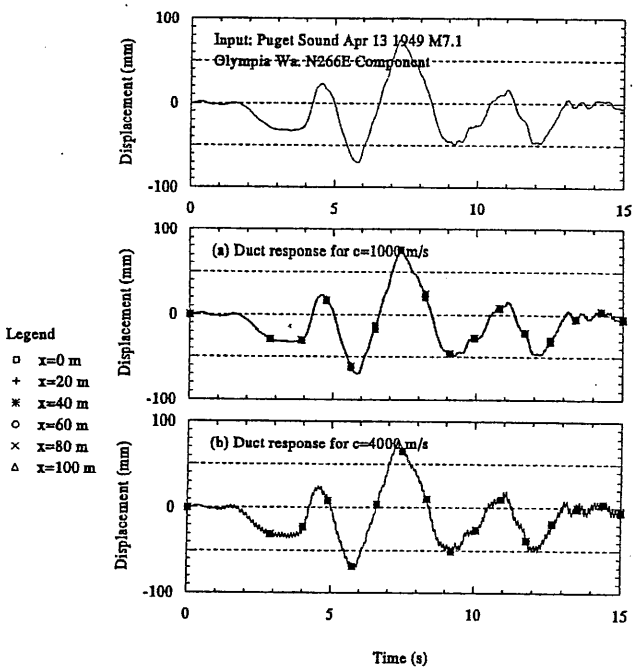

Fig. 10. Steel pipe axial displacement response to the San Fernando earthquake displacement time history at equally spaced locations along a 100 m duct section and considering two propagation velocities. The zero lag (x=0) input time history is also shown.

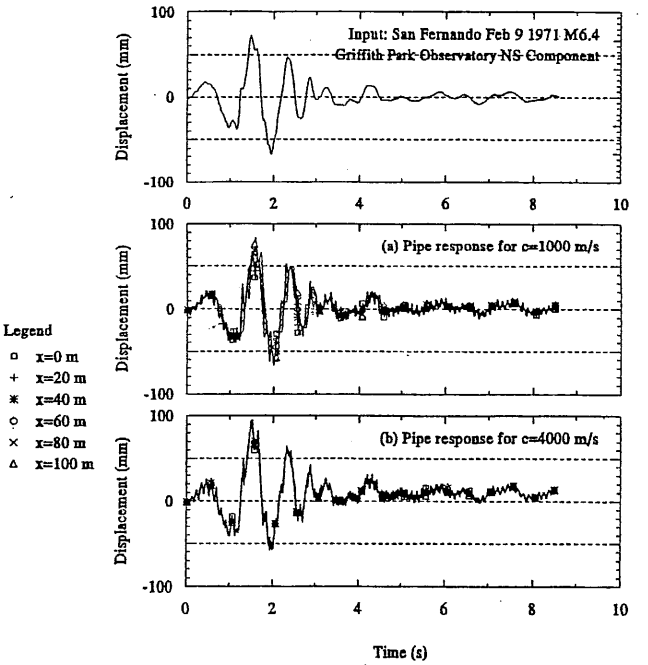

Fig. 11. Steel pipe axial displacement response to the Olympia, Wa. earthquake displacement time history at equally spaced locations along a 100 m duct section and considering two propagation velocities. The zero lag (x=0) input time history is also shown.

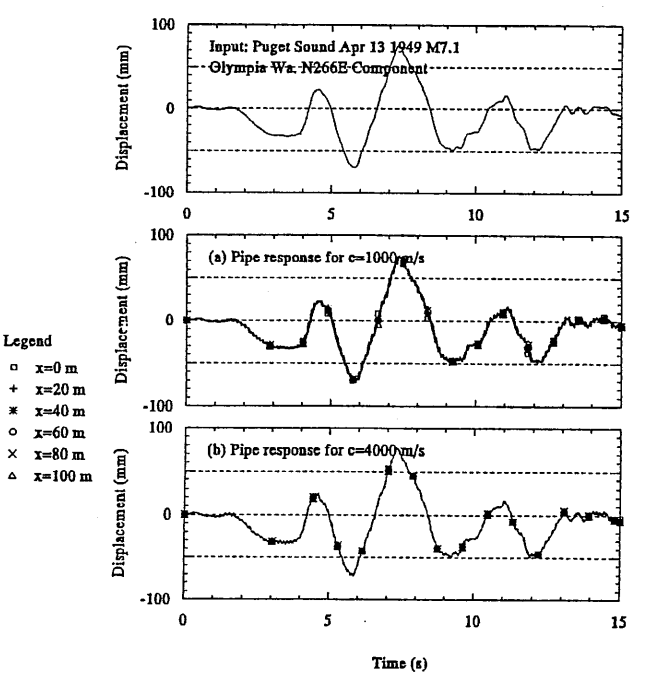

Internal Problem

Dynamic analyses have been carried out to assess axial displacements and forces induced in cables along selected circuits in the Vancouver Lower Mainland. The dynamic modeling of one particular circuit is presented herein. A 700 m long section of cable was modelled having a variable slope of up to 3° and containing one manhole connection point (M127C) near the mid-point of the model. Three copper conductor cables are placed in pipes, approximately 206 mm in diameter. Sections of cable are connected by joints in larger diameter pipe contained within each manhole.

All points along the model were assumed free to move in response to applied ground motion input. Cable properties (area, Young's modulus, mass per unit length, yield stress in tension and compression) and the estimated coefficient of friction between the cable and pipe were supplied by BC Hydro. Since three cables were put in one pipe, structural properties were set equal to 3 times those of an individual cable.

Displacement time histories at stations I-06, C-00 and I-12 from the SMART array were used as free field input into the cable analysis. It was assumed that the manhole tracked with the external free field ground displacements. The assumed propagation velocity, 2800 m/sec, was used to compute time lags for input ground displacements at various spring support points between each of the stations.

To model the cable-manhole connection point, an axial spring element was used to link adjacent cable segments. The connector element was assumed to be capable of withstanding tension but unable to withstand compression.

Assuming a coefficient of friction equal to 0.17 and no slack in the cable connector at the manhole location, the axial displacement time histories of the cable relative to the external pipe at three locations along the cable are shown at the top of Fig.12. Approximately 50 mm of downhill movement is seen to occur relative to the pipe under the influence of the initial gravitational forces imposed prior to the start of shaking. Yielding of the cable-pipe interaction springs occurred, resulting in slip between the cable and pipe. The corresponding axial forces in the joint element at the manhole connection point are shown at the bottom of Fig.12.

Fig. 12. Response of an internal cable section to a travelling seismic wave

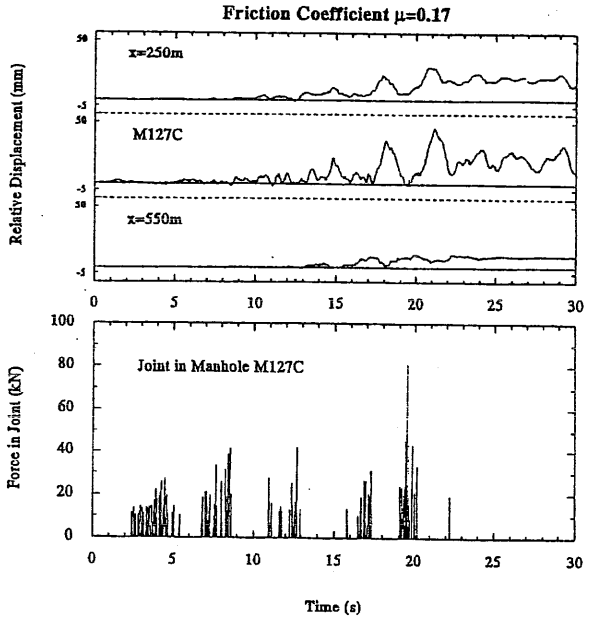

It is noted that the large magnitude of the induced forces (80 kN) is due to the assumption of zero slack in the joint element, or at any point along the cable. For the case shown, if a slack of 50 mm was assumed, the induced forces would be approximately zero.

From similar analyses carried out on other BC Hydro circuits incorporating variable slope configurations and cable-manhole layouts the following additional comments are made:

- Significant tensile axial forces can be induced in cables at manhole connection points due to passage of moderate amplitude (± 100 mm) seismic wave trains.
- The magnitude of axial force in the cables at manhole connection points can be reduced substantially through introduction of an initial slack in the system.
- The magnitude of axial force at cable connection points is found to decrease with decrease in friction between the cable and cable duct, as well as with the assumption that manholes follow completely the input ground motion.
- The magnitude of relative displacements across the cable connectors depends strongly on the amplitude and spatial variation of input ground displacements, as well as whether manholes are assumed to fully resist or move in phase with the input ground motions.

- The magnitude of peak axial forces and relative displacements will depend strongly on cable slope and cable weight per unit length, amplitude and spatial distribution of input ground displacements applied to the cable, frictional characteristics of the cable-cable duct interface, and cable connection details within manholes.

Conclusions

Based on the analyses carried out, the following conclusions have been drawn:

(1) Two dimensional models for computing the dynamic response of transmission cables installed in ducts or pipes have been successfully developed.

(2) Preliminary modelling of the response of the external pipe (duct) to travelling ground waves indicated that the pipe moved essentially with the ground so that it was reasonable to apply "free field" ground displacements as dynamic input to model cable - pipe interaction.

(3) Assumptions as to whether manholes track with or resist the free field ground displacements can have a large impact on computed internal cable response.

(4) Factors affecting the dynamic response of cables in ducts and pipes include displacement ground motion input (amplitude, frequency content and time lag), angle and length of slope, coefficient of cable-pipe friction, cable mass/stiffness properties and availability of slack in the cables.

(5) Assuming manholes and external cable ducts (or pipes) track fully with the free field ground displacements, the analyses predict that excessive forces can be set up in the cables at joint connectors depending on characteristics of the input ground motions, cable properties and installation conditions. Where manholes are assumed to resist the free field ground displacements, axial cable forces can be further increased.

Acknowledgements

The authors wish to acknowledge the permission of BC Hydro to publish the results of this work. The work was carried out while Drs. Gohl and Dunbar were employees of Agra Earth and Environmental (AEE) Ltd. The authors wish also to thank AEE for permission to publish this work.

References

Audibert, J.M.E., Nyman, D.J., and O'Rourke, T.D. 1984. Differential Ground Movement Effects on Buried Pipelines. *In* Guidelines for the Seismic Design of Oil and Gas Pipeline Systems, ASCE Technical Council on Lifeline Earthquake Engineering.

Bolt, B.A., Loh, C.H., Penzien, J., Tsai, Y.B., and Yeh, Y.T. 1982. Preliminary Report on the SMART-1 Strong Motion Array in Taiwan. *In* Report UCB/EERC-82/13, University of California, Berkeley.

Hadjian, A.H. and Hadley, D.M. 1981. Studies of Apparent Seismic Wave Velocity. *In* International Conference on Recent Advances in Geotechnical Engineering and Soil Dynamics, St. Louis, Mo.

Hao, H., Oliveira, C.S. and Penzien, J. 1989. Multiple Station Ground Motion Processing and Simulation Based on SMART-1 Array Data. *In* Nuclear Engineering and Design, vol. 111, pp. 293-310.

Loh, C.H. 1985. Analysis of the Spatial Variation of Seismic Waves and Ground Movements for SMART-1 Array Data. *In* Earthquake Engineering and Structural Dynamics, vol. 13, pp. 561-581.

O'Rourke, M.J. and El Hmadi, K. 1988. Analysis of Continuous Buried Pipelines for Seismic Wave Effects. *In* Earthquake Engineering and Structural Dynamics, vol. 16, pp. 917-1929.

Prakash, V., Powell, G.H., and Campbell, S. 1993. DRAIN-2DX Base Program Description and User Guide. *In* Report UCB/SESM-93-16, Dept. of Civil Engineering, University of California, Berkeley.